Clathrin plaques and associated actin anchor intermediate filaments in skeletal muscle

Agathe Franck[a], Jeanne Lainé[a,b], Gilles Moulay[a], Eline Lemerle[a], Michaël Trichet[c], Christel Gentil[a], Sofia Benkhelifa-Ziyyat[a], Emmanuelle Lacène[d], Mai Thao Bui[d], Guy Brochier[d], Pascale Guicheney[e], Norma Romero[a,d], Marc Bitoun[a], and Stéphane Vassilopoulos[a,*]

[a]Center of Research in Myology, Institute of Myology, UMRS 974, INSERM, Sorbonne Université, F-75013 Paris, France; [b]Department of Physiology, Pitié-Salpêtrière Hospital, Sorbonne Université, F-75013 Paris, France; [c]Institut de Biologie Paris-Seine, Sorbonne Université, CNRS, FR3631 Paris, France; [d]Neuromuscular Morphology Unit, Institute of Myology, Pitié-Salpêtrière Hospital, Sorbonne Université, F-75013 Paris, France; [e]Institute of Cardiometabolism and Nutrition, UMRS 1166, INSERM , Sorbonne Université, F-75013 Paris, France

ABSTRACT Clathrin plaques are stable features of the plasma membrane observed in several cell types. They are abundant in muscle, where they localize at costameres that link the contractile apparatus to the sarcolemma and connect the sarcolemma to the basal lamina. Here, we show that clathrin plaques and surrounding branched actin filaments form microdomains that anchor a three-dimensional desmin intermediate filament (IF) web. Depletion of clathrin plaque and branched actin components causes accumulation of desmin tangles in the cytoplasm. We show that dynamin 2, whose mutations cause centronuclear myopathy (CNM), regulates both clathrin plaques and surrounding branched actin filaments, while CNM-causing mutations lead to desmin disorganization in a CNM mouse model and patient biopsies. Our results suggest a novel paradigm in cell biology, wherein clathrin plaques act as platforms capable of recruiting branched cortical actin, which in turn anchors IFs, both essential for striated muscle formation and function.

INTRODUCTION

For vesicle formation, triskelia composed of trimerized clathrin heavy chains (CHCs) with bound clathrin light chains, are recruited by clathrin adaptors that trigger clathrin-coated vesicle budding (Brodsky, 2012; Robinson, 2015). The adaptor proteins are required for targeting clathrin to specific intracellular compartments, and among these, adaptor protein 2 (AP2) recruits clathrin to the plasma membrane (PM). In several cell types, and notably in skeletal muscle myotubes, flat clathrin plaques cover large portions of the PM (Heuser, 1980; Maupin and Pollard, 1983; Saffarian et al., 2009; Taylor et al., 2011; Grove et al., 2014; Dambournet et al.,

2018). Although flat clathrin lattices are thought to be a structural intermediate that will bud to form a canonical coated pit, the role of these extensive flat clathrin plaques in specific differentiated cell types remains elusive. They are invariably associated with the actin cytoskeleton (Heuser, 1980; Saffarian et al., 2009; Vassilopoulos et al., 2014; Leyton-Puig et al., 2017); they mediate adherence to the extracellular substrate through integrins such as β5-integrin (De Deyne et al., 1998; Vassilopoulos et al., 2014; Lampe et al., 2016); and they are thought to serve as hot spots for endocytosis, because budding pits are frequently observed at their periphery

(Taylor *et al.*, 2011; Lampe *et al.*, 2016). Dynamin 2 (DNM2), a large GTPase that acts as a mechanochemical scaffolding molecule that releases nascent vesicles from the PM or intracellular compartments (van Dam and Stoorvogel, 2002; Kaksonen and Roux, 2018), is a bona fide clathrin plaque component (Grove *et al.*, 2014). In addition, several studies have demonstrated that DNM2 regulates actin cytoskeleton networks and have proposed functions for dynamin in actin polymerization that are distinct from coated vesicle formation (Schafer *et al.*, 2002; Orth and McNiven, 2003; Saffarian *et al.*, 2009; Gu *et al.*, 2010; Bonazzi *et al.*, 2012; González-Jamett *et al.*, 2017). Mutations in the *DNM2* gene cause autosomal dominant centronuclear myopathy (CNM) (Bitoun *et al.*, 2005), a slowly progressive congenital myopathy characterized by muscle weakness, hypotonia, and the presence of centrally located nuclei in a large number of muscle fibers in the absence of regenerative processes.

In skeletal muscle, CHC and DNM2 are localized at specific PM sites called costameres. Clathrin depletion in vivo leads to drastic detachment of the peripheral contractile apparatus from the PM and decreased force (Vassilopoulos et al., 2014). Costameres correspond to lateral contacts between the PM and the contractile apparatus (Pardo *et al.*, 1983a,b; Shear and Bloch, 1985) and play a pivotal role in integrating adhesion with the propagation of forces (Danowski *et al.*, 1992). They are composed of large membrane protein complexes, that is, the focal adhesion complex and the dystrophin–glycoprotein complex, which are both linked to the contractile apparatus by actin and desmin intermediate filaments (IFs) (Ervasti, 2003). Desmin is a muscle-specific, type III IF protein, well documented for its role in cell architecture and force transmission (Herrmann *et al.*, 2007; Capetanaki *et al.*, 2015), which forms a stress-transmitting network involved in signaling, mechanotransduction, and gene expression (Palmisano *et al.*, 2015). Although it is established that mechanical cues sensed by costameres are transduced into biochemical signals leading to sarcomere assembly and gene expression regulation, little is known on the specific mechanisms involved.

Here, we set out to elucidate the composition of clathrin plaques in differentiated myotubes and to understand the contribution of plaque defects to costamere disorganization in CNM. By combining multimodal microscopy on small interfering RNA (siRNA)-depleted myotubes and by analyzing DNM2 knock-in (KI) mice and CNM human biopsies, we report that CHC, DNM2 and branched actin filaments compose a membrane microdomain that is required to anchor desmin IFs at the myotube surface. We show that the *DNM2* mutations that are responsible for CNM in humans deregulate the actin-clathrin cross-talk and subsequently disorganize the desmin network.

RESULTS
### Clathrin plaques act as platforms for cytoskeletal organization
We analyzed clathrin plaques from extensively differentiated primary mouse myotubes. At the light microscopy level, clathrin-positive fluorescent patches aligned along the lateral PM and were spaced apart by 2 ± 0.5 µm (Figure 1A). We developed an unroofing procedure coupled to metal-replica electron microscopy (EM) aimed at visualizing these structures en face from differentiated myotubes. Platinum replicas obtained from primary mouse myotubes presented spaced clathrin plaques surrounded by cortical cytoskeletal filaments (Figure 1, B–D). Three-dimensional (3D) organization and composition of cytoskeletal components surrounding clathrin plaques were defined by a combina-

tion of platinum-replica EM and electron tomography either by producing stereoscopic 3D anaglyphs (Figure 1D) or by collecting tomograms at tilt angles up to ±25° with 5° increments relative to the plane of the sample (Supplemental Movie 1). The small clusters of branched actin around clathrin plaques formed a shell around thicker filaments emanating from surrounding stress fibers (Supplemental Figure 1, A and B). Previous studies suggested receptor-mediated endocytosis can be actin dependent via Arp 2/3 branched actin filaments (Yarar *et al.*, 2005; Kaksonen *et al.*, 2006; Collins *et al.*, 2011). In agreement with our ultrastructural analysis showing branched actin around clathrin plaques, we detected ArpC2, a component of the Arp2/3 complex, on actin filaments surrounding clathrin plaques (Supplemental Figure 1, C and D). This result is in agreement with the role of actin polymerization promoted by Arp2/3 in the regulation of clathrin plaques (Leyton-Puig *et al.*, 2017). Measurement of filament diameter allowed us to discriminate between straight and thin 10 nm on-average actin filaments versus thicker 15 nm filaments (including metal coating; Supplemental Figure 1G). Immunogold labeling confirmed that this 3D network is composed of IFs positive for desmin that directly connect actin stress fibers and branched actin "nests" around flat clathrin plaques (Figure 1F and Supplemental Figure 1, E and F). We tested whether clathrin plaques were involved in cortical desmin network organization by performing siRNA-mediated knockdown in differentiated myotubes. CHC depletion was performed on multinucleated myotubes to avoid potential interference with the differentiation process using validated sequences (Ezratty *et al.*, 2009; Vassilopoulos *et al.*, 2014). We noticed that CHC depletion consistently induced the aggregation of desmin in the cytoplasm (Figure 2, A and B). The desmin aggregates in the cytoplasm of primary CHC-depleted muscle cells resembled the aggregates found in muscle cells from patients with desminopathies and were composed of either small desmin-positive spots or larger aggregates reaching several microns in diameter. To test whether the clathrin-depletion phenotype was due to clathrin recruited specifically at the PM, we depleted the α-subunit of the AP2 adaptor. AP2 depletion phenocopied clathrin depletion and induced the formation of desmin aggregates in the cytoplasm (Figure 2C). Depleting AP1 (γ-subunit) or AP3 (δ-subunit) involved in the recruitment of clathrin to the Golgi apparatus and endosomal systems, respectively, had no effect on desmin distribution (Figure 2C). To firmly demonstrate that clathrin plaques and not clathrin-mediated endocytosis were involved in IF aggregation, we depleted β5-integrin, whose requirement for clathrin plaque formation has been established (De Deyne *et al.*, 1998; Zuidema *et al.*, 2018). Depletion of β5-integrin in differentiated mouse myotubes led to reduced clathrin patches on the myotube membrane and strong aggregation of desmin in the cytoplasm (Figure 2, C and D). Thin-section EM on CHC- or AP2-depleted myotubes confirmed that the aggregates were composed of IF tangles (Figure 2, G–L).

Branched actin surrounding clathrin plaques is regulated by DNM2 and neural Wiskott–Aldrich syndrome protein and organizes desmin IFs
Given DNM2's function in actin remodeling, we reasoned that it could organize branched actin filaments, including those surrounding clathrin plaques that anchor IFs.

DNM2-depleted myotubes consistently presented increased clathrin patches on the myotube's lateral membrane (Figure 3, A and B), many desmin aggregates in the cytoplasm (Figure 3, A
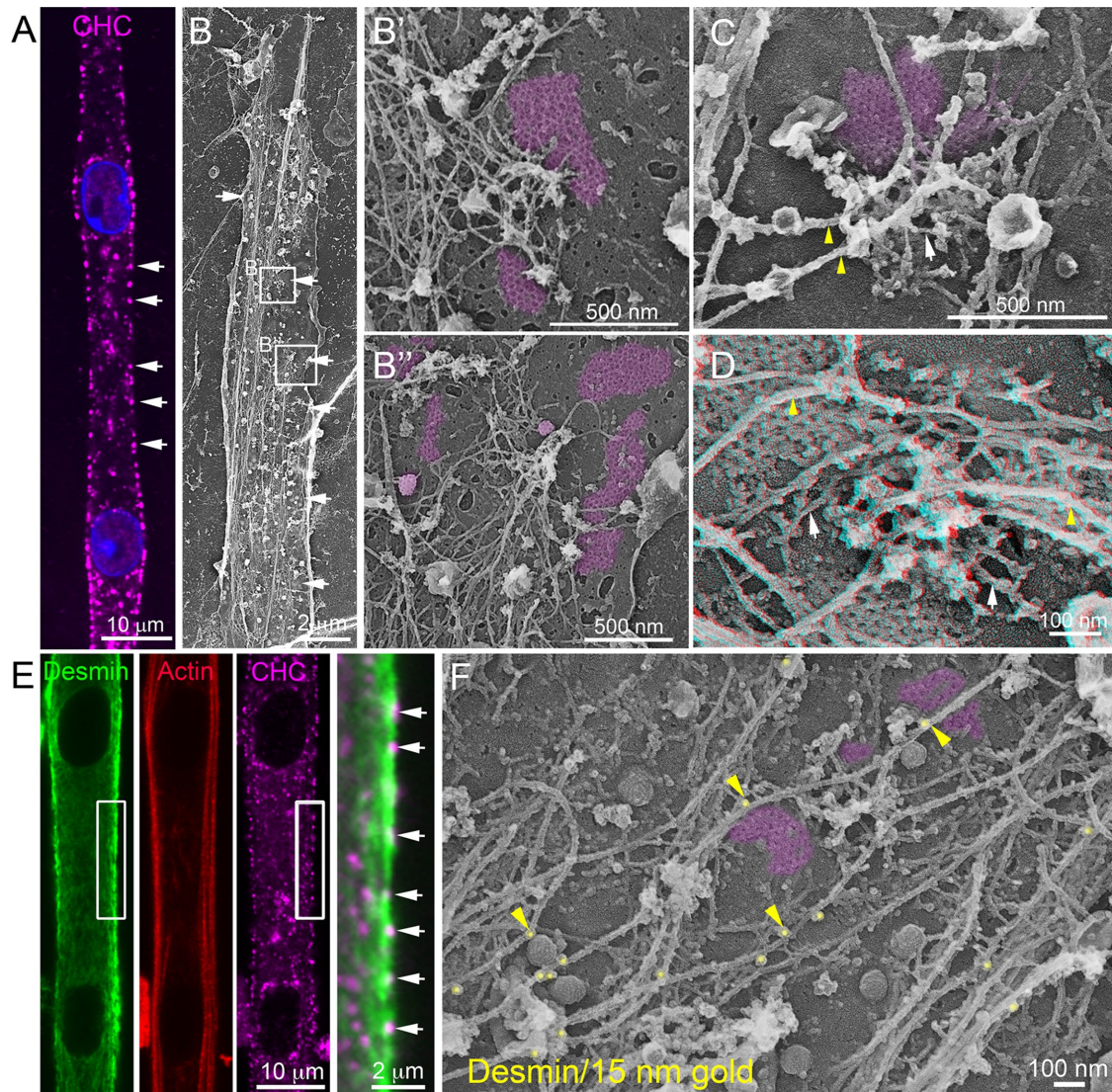
FIGURE 1: Clathrin-coated plaques anchor desmin IFs. (A) Immunofluorescent staining of CHC (magenta) in differentiated mouse primary myotubes. (B) Survey view of an unroofed primary mouse myotube. (B′, B″) Higher-magnification views corresponding to the boxed regions in B. (C, D) Higher-magnification views of clathrin plaques and associated cytoskeletal structures in unroofed control primary myotubes. Intermediate filaments are indicated with yellow arrowheads and actin filaments are indicated using arrows. For D, use glasses for 3D viewing of anaglyph (left eye = red). (E) Immunofluorescent staining of desmin (green), actin (red), and CHC (magenta) in mouse primary myotubes. (F) Higher-magnification view of clathrin plaques and associated cytoskeletal structures in unroofed control primary myotubes immunolabeled using a primary antibody against desmin and secondary antibodies coupled to 15 nm gold beads. Images are representative of at least four independent experiments. Gold beads are pseudocolored in yellow, and some are indicated with yellow arrowheads. Clathrin-coated structures are highlighted in purple.

and C), decreased cortical actin labeling (Figure 3D), and dispersed α-actinin 2 clusters in the cytoplasm that corresponded to abnormal Z-bands (Supplemental Figure 2, E–H). Ultrastructural analysis of DNM2-depleted myotubes indicated altered morphology of branched actin nests surrounding clathrin plaques, mostly composed of small actin filaments associated with an accumulation of proteinaceous material (Figure 3E and Supplemental Figure 4). We next performed thin-section EM to detect abnormal IF tangles in the DNM2-depleted myotubes corresponding to desmin aggregates (Figure 3, D–H) and were able to visualize dense IF tangles in DNM2-depleted cells by metal-replica EM, as these were still associated to the PM and resisted sonication shear forces produced during unroofing (Figure 3H). These aggregates also

contained small heat-shock protein αB-crystallin and some ArpC2, although they excluded actin (Figure 3D and Supplemental Figure 2I). Neural Wiskott–Aldrich syndrome protein (N-WASP) is directly involved in the generation of Arp2/3 branched actin filaments during endocytosis and a known DNM2 indirect partner (Merrifield *et al.*, 2004). In agreement, we observed an interaction between DNM2 and N-WASP and some desmin in mouse primary myotubes upon DNM2 immunoprecipitation (Supplemental Figure 3). N-WASP depletion induced desmin aggregates similar to those produced by DNM2 and CHC depletion (Figure 4, A and C, and Supplemental Figure 5) and decreased cortical actin labeling (Figure 4B). Upon EM inspection, N-WASP depletion produced accumulation of small actin filaments with the same proteinaceous
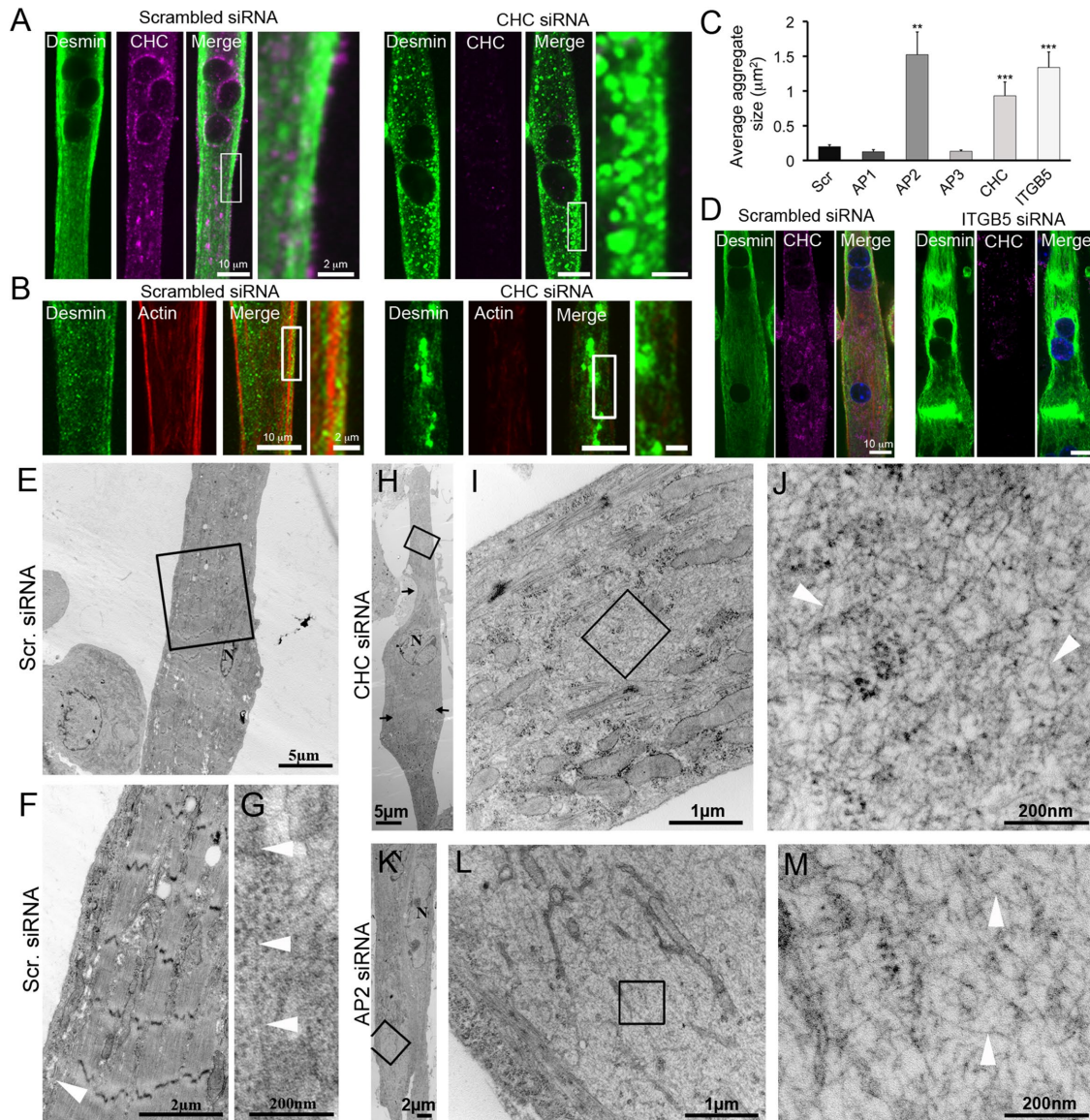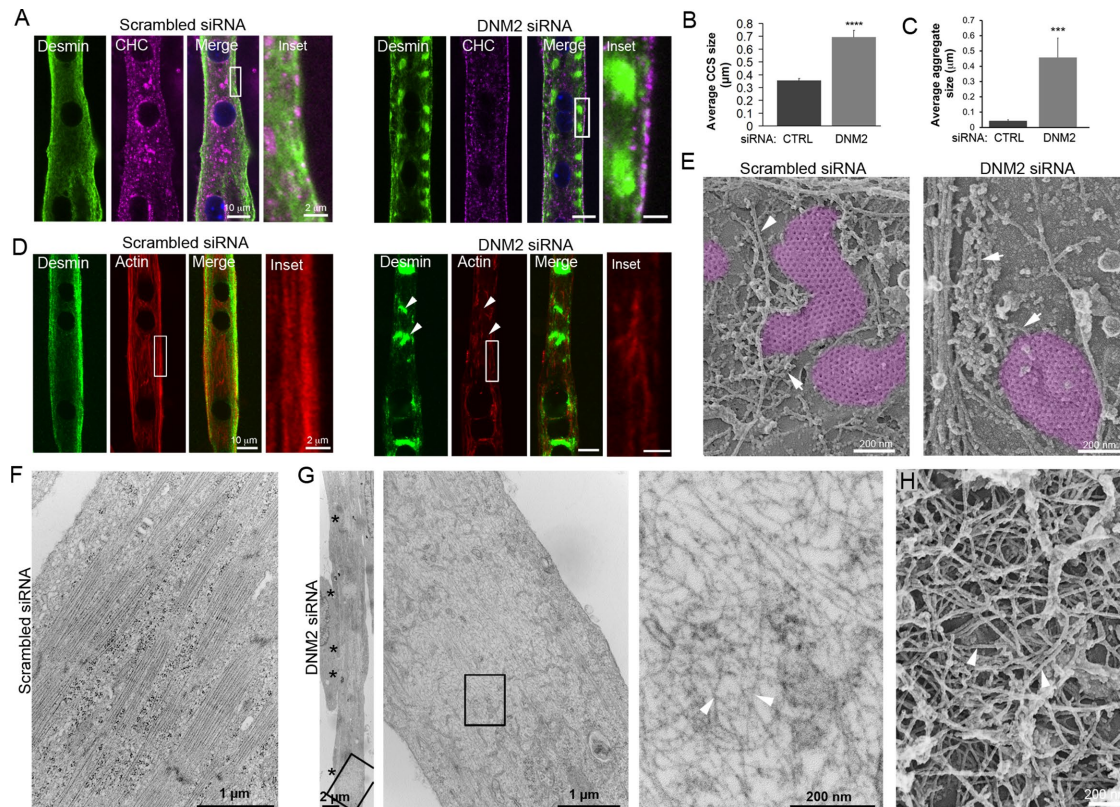
FIGURE 2: Clathrin-coated plaques are required for desmin IF organization. (A) Immunofluorescent staining of desmin (green) and CHC (magenta) in mouse primary myotubes treated with control or CHC siRNA. Images are representative of at least 10 independent experiments. (B) Desmin (green) and actin staining (red) in mouse primary myotubes treated with control or CHC siRNA. (C) Average desmin aggregate size in myotubes treated with control siRNA or siRNA against CHC, AP1, AP2, AP3, or β5 integrin (ITGB5) ($n = 30$–50 myotubes). Data presented as mean $\pm$ SEM; **, $p < 0.01$, ***, $p < 0.001$ using a two-tailed Student's t test). (D) Immunofluorescent staining of desmin (green) and CHC (magenta) in mouse primary myotubes treated with control or ITGB5 siRNA. (E–L) Thin-section EM of primary myotubes treated with control (E–G), CHC (H–J), or AP2 (K–M) siRNA. I and L are higher-magnification views of IF tangles from H and K, respectively. Images are representative of at least two to four independent experiments. IFs are indicated with arrowheads.

material observed upon DNM2 depletion (Figure 4E and Supplemental Figure 5).

Clathrin plaques and cortical actin are altered in desmin knockout mice

We next tested whether the presence of the cortical desmin IF web could contribute in stabilizing clathrin plaques and the surrounding branched actin structures by culturing primary myotubes from desmin knockout mice (desmin$^{-/-}$). At the light microscopy resolution, desmin$^{-/-}$ myotubes displayed some clathrin patches at the myotube membrane (Figure 5A) but had significantly reduced cortical

and total actin labeling (Figure 5, A–C), suggesting that the presence of desmin IFs is necessary to stabilize cortical actin. Upon inspection at the EM level, the clathrin patches in the desmin$^{-/-}$ myotubes were often composed of many coated-pit clusters (Figure 5, D–F). Morphometric analysis of the structures present in metal replicas from desmin$^{-/-}$ myotubes confirmed a significant reduction of the size and total surface occupied by flat clathrin-coated structures at the expense of increased canonical clathrin-coated pits. Altogether, these data demonstrate that clathrin is required in the first instance to organize actin and recruit desmin, but that after that initial event, desmin stabilizes the clathrin-associated actin.
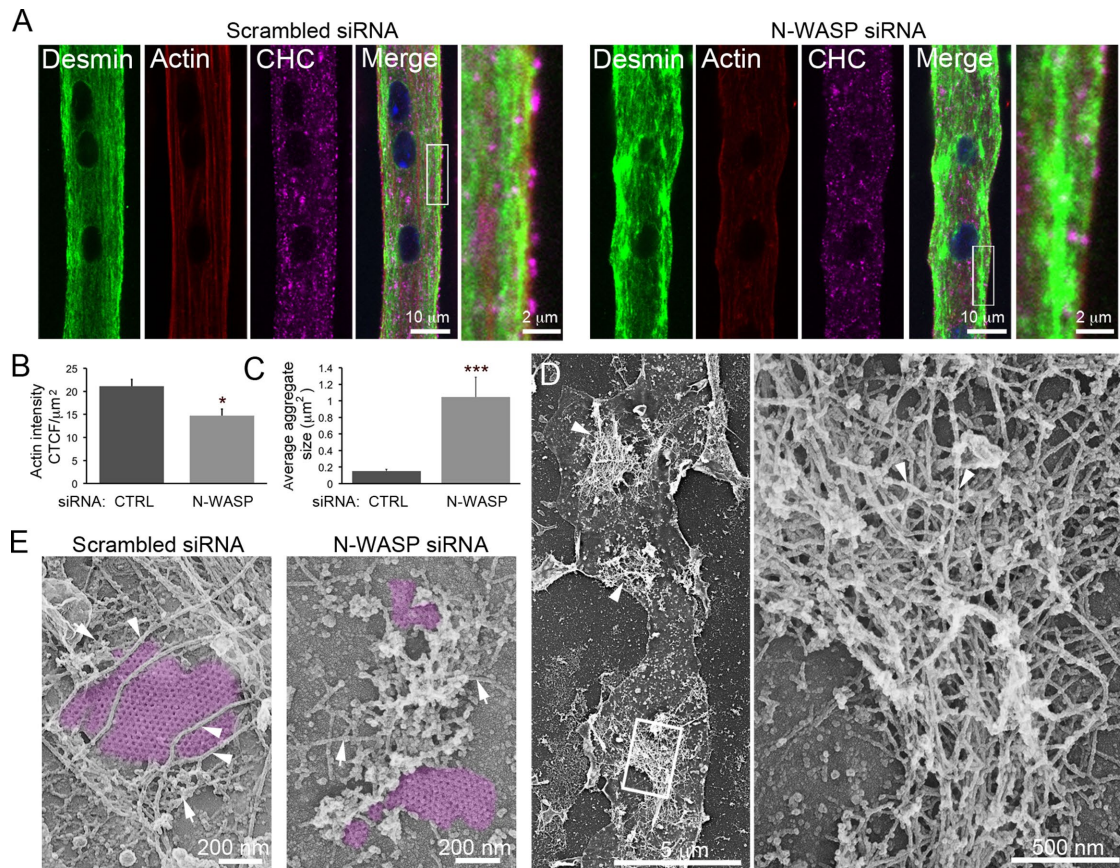
FIGURE 3: DNM2 is required for desmin and actin organization around clathrin plaques. (A) Immunofluorescent staining of desmin (green) and actin (red) in mouse primary myotubes treated with control or DNM2 siRNA. Images are representative of at least seven independent experiments. (B) Average clathrin-coated structure (CCS) size in myotubes treated with control or siRNA against DNM2 ($n = 20$ myotubes). (C) Quantification of desmin aggregate fluorescence in myotubes treated with control or DNM2 siRNA ($n = 20$ myotubes). (D) Desmin (green) and actin staining (red) in mouse primary myotubes treated with control or DNM2 siRNA. (E) High-magnification view of unroofed primary mouse myotubes treated with control or DNM2 siRNA. Actin structures are indicated using arrows. Images are representative of at least 12 independent experiments. (F, G) Thin-section EM of extensively differentiated control (F) or DNM2-depleted (G) myotubes. Images are representative of at least eight independent experiments. Arrowheads denote bone fide IFs. (H) High-magnification view of a desmin aggregate from unroofed primary mouse myotubes treated with DNM2 siRNA. Data are presented as mean ± SEM; ***, $p < 0.001$, ****, $p < 0.0001$, using a two-tailed Student's t test.

DNM2-linked CNM mutations disorganize clathrin plaques and desmin in vivo

The involvement of DNM2 prompted us to analyze clathrin plaques and the desmin network in *DNM2*-related CNM. We first analyzed clathrin plaques in a knock-in mouse model for the most frequent human mutation, that is, heterozygous (HTZ) KI-*Dnm2*R465W mice. Given that the AP2 adaptor is specifically recruited at the PM and is a bona fide component of clathrin plaques in muscle, it was used as marker to study the plaques in vivo. We transduced the tibialis anterior (TA) muscle with an adeno-associated virus (AAV9) expressing the µ2-subunit of the AP2 clathrin adaptor tagged with mCherry (AP2-mCherry). In wild-type (WT) mice, AP2-mCherry was expressed at the surface of muscle fibers; aligned with the Z-bands; and colocalized with endogenous AP2, CHC, DNM2, and α-actinin 2 (Supplemental Figure 6). In HTZ KI-*Dnm2*R465W mice, AP2 distribution was discontinuous, and AP2 patches were completely disorganized in the most severely affected regions (Figure 6A and Supplemental Figure 6, A–D). Because DNM2 participates in cytoskeletal organization and flat clathrin plaque homeostasis in vitro, we reasoned that CNM-causing mutations could induce defects in PM IF organization and lead to malfunction of muscle costameres in vivo. We investigated the organization of the desmin network in dissociated fibers from HTZ KI-*Dnm2*R465W mice.

Confocal sections from the top to the bottom of dissociated fibers revealed disorganization of desmin distribution at the surface of isolated fibers from HTZ KI-*Dnm2*R465W mice (Figure 6B). Analysis of muscle from HTZ KI-*Dnm2*R465W mice using thin-section EM revealed the presence of large regions of the surface containing IF tangles (Figure 6, D–F), resembling those observed in CHC-, AP2- and DNM2-depleted myotubes. These characteristic aggregates were also present around central nuclei in HTZ KI-*Dnm2*R465W mice (Figure 6, H and I).

The results from *DNM2* knock-in mice prompted us to investigate the organization of desmin IFs in CNM patients with *DNM2* mutations. Muscle biopsies from DNM2-related CNM patients present a characteristic radial arrangement of sarcoplasmic strands particularly visible with oxidative enzyme reactions. Transverse muscle sections from patients harboring either the p.R465W or the p.R369Q *DNM2* mutation presented a strong desmin accumulation in the radiating sarcoplasmic strands, typical of dilated Z-band material, which stretched from central nuclei toward the sarcolemma (Figure 7, A–D). At the EM level, central nuclei appeared to have no morphological abnormality, and the radial distribution of the intermyofibrillar sarcoplasmic strands was easily recognized. These radial strands contained dense protein accumulations, typical of dilated Z-band material (Figure 7E).

FIGURE 4: N-WASP is indispensable for desmin and actin organization around clathrin plaques. (A) Immunofluorescent staining of desmin (green), CHC (magenta), and actin (red) in mouse primary myotubes treated with control or N-WASP siRNA. Images are representative of at least five independent experiments. (B) Quantification of cortical actin fluorescence intensity in myotubes treated with control or N-WASP siRNA ($n = 20$ myotubes). (C) Quantification of desmin aggregate size in myotubes treated with control or N-WASP siRNA ($n = 20$ myotubes). (D) Survey view of desmin aggregates (arrowheads) from unroofed primary mouse myotubes treated with N-WASP siRNA. (E) High-magnification views of unroofed primary mouse myotubes treated with control or N-WASP siRNA. IFs are indicated with arrowheads, and actin structures are indicated using arrows. Images are representative of at least five independent experiments. Data are presented as mean ± SEM; *, $p < 0.05$, ***, $p < 0.001$, using a two-tailed Student's t test.

DISCUSSION

Collectively, our experiments show the existence of a compartment centered on clathrin plaques and surrounded by branched actin networks forming a link between the extracellular matrix and IFs. By virtue of shaping both clathrin lattices and branched actin filaments, DNM2 takes center stage as a key regulator of these structures. Comparable to focal adhesions, clathrin plaques are macromolecular functional units that connect extracellular matrix and intracellular cytoskeleton at the PM. Our work shows that branched actin filaments that form around adhesive clathrin plaques are the central element for IF anchoring, and we confirm that DNM2 and N-WASP are central actors of actin remodeling at these sites (Supplemental Figure 7). We have previously shown that the actin network surrounding clathrin lattices contains α-actinin 2, an actin cross-linking protein (Vassilopoulos et al., 2014). It is of interest that hybrid Arp2/3 and α-actinin–containing complexes have already been reported (Chorev et al., 2014; Pizarro-Cerdá et al., 2017) and association of clathrin plaques with these tissue-specific hybrid complexes could be the signature of clathrin's role in adhesion and association with the cytoskeleton. DNM2, previously shown by EM to associate with flat clathrin structures (Damke et al., 1994; Warnock et al., 1997; Sochacki et al., 2017), interacts with the cellular machinery, including

N-WASP, that induces branched actin polymerization around clathrin plaques. We also provide the first evidence that IFs of desmin, prominent in cells subject to mechanical stress and capable of connecting the cell surface with peripheral nuclei, can associate with actin structures surrounding clathrin plaques. Depleting either bona fide plaque components or branched actin formation induced IF aggregates such as those found in patients with desmin mutations (Clemen et al., 2015), underscoring the strong dependence of cortical IF organization on clathrin plaques and associated actin machinery. These results suggest a requirement for clathrin to organize branched actin and recruit desmin IFs, but it is also possible that desmin IFs could stabilize the clathrin-associated branched actin structures. In agreement, absence of desmin IFs in the desmin$^{-/-}$ mice allows formation of clathrin plaques associated with actin cytoskeleton but leads to reduced plaques and subsequent increased budding. One intriguing possibility could be that, when branched actin filament bundles are involved in interactions with IFs, they are less available for promoting endocytosis. In addition, one cannot rule out that other IFs may also regulate the spatial organization of clathrin plaques and neighboring actin networks.

DNM2 mutations causing the autosomal dominant CNM mostly segregate in the middle domain involved in DNM2 oligomerization
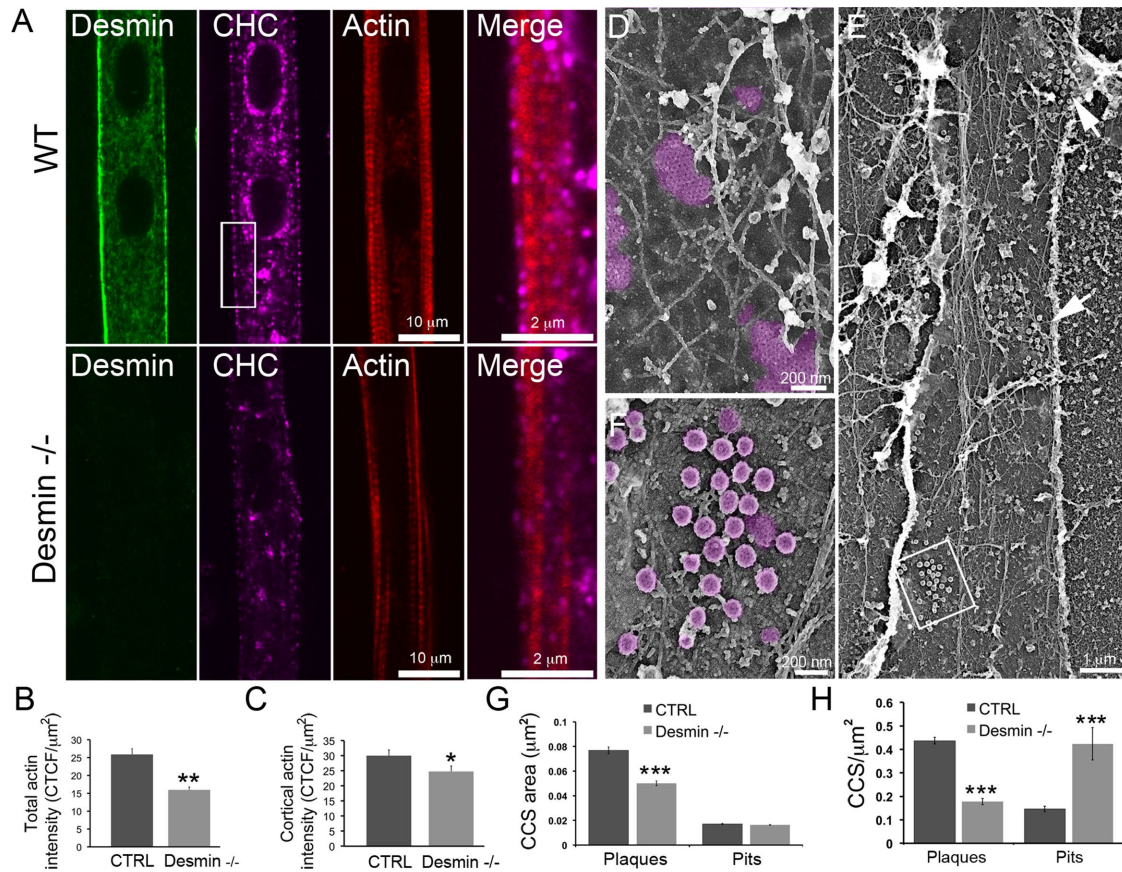
FIGURE 5: Clathrin plaques and actin are altered in desmin knockout mice. (A) Immunofluorescence detection of desmin (green), CHC (magenta), and actin staining (phalloidin, red) in WT or desmin knockout (desmin$^{-/-}$) mouse myotubes. Scale bars: 10 μm; 2 μm (insets). (B) Quantification of total actin fluorescence intensity in WT or desmin knockout$^{-/-}$ myotubes ($n = 18$–21 myotubes). (C) Quantification of cortical actin fluorescence intensity in WT or desmin knockout mice myotubes ($n = 18$–21 myotubes). (D) High-magnification view of an unroofed primary mouse myotube from WT mice. (E) Survey view of an unroofed desmin$^{-/-}$ myotube. Arrows indicate clathrin-coated pit accumulations. (F) Higher-magnification view corresponding to the boxed region in E. (G) Morphometric analysis of clathrin-coated structure size from WT or desmin knockout mouse myotubes. (H) Morphometric analysis of clathrin-coated structure density per membrane surface from WT or desmin$^{-/-}$ myotubes. Images are representative of at least five independent experiments. Data are presented as mean ± SEM; *, $p < 0.05$, **, $p < 0.01$, ***, $p < 0.001$, using a two-tailed Student's t test.

and actin remodeling (Durieux *et al.*, 2010; González-Jamett *et al.*, 2017). This domain has been shown to directly interact with actin, and it is highly probable that the CNM phenotype observed in patients with DNM2 mutations directly stems at least in part from defective cortical actin turnover. These defects would produce dysfunctional force transmission at costameres, explaining reduced force generation in muscle from the KI-*Dnm2*^{R465W} mouse model (Durieux *et al.*, 2010). Mechanistic understanding of CNM pathophysiology stemming directly from this work concerns the interplay between nuclear positioning and the IF tangles described here. The link between desmin IFs with both PM and peripheral nuclei in muscle is well established, and it was recently shown that Arp2/3 and actin organize desmin for peripheral nuclear positioning (Roman *et al.*, 2017). Our results suggest the peculiar organization termed "radial sarcoplasmic strands," found in CNM patient fibers, is a consequence of the desmin tangles systematically forming at the surface and around nuclei. The desmin tangles could adopt the radiating appearance characteristic of this disease during nuclear centralization. Importantly, the clathrin plaque–based structure may be the Achilles' heel of several tissues, and its dysfunction may lead to additional disorders, including cancer, where abnormal clathrin

plaque assembly or misregulated DNM2 function could perturb the fine coupling between adhesion and force sensing.

MATERIALS AND METHODS

Antibodies
Primary antibodies are listed in Supplemental Table 2. Secondary antibodies for immunofluorescence were Alexa Fluor 488, Alexa Fluor 568, and Alexa Fluor 647 conjugates (Life Technologies, France). Secondary antibodies for Western blotting were coupled to horseradish peroxidase (HRP; Jackson Laboratories, USA). Secondary antibodies used after immunoprecipitation were Trueblot immunoglobulin G (IgG) HRP from Rockland, USA.

Mouse myoblast cultures and siRNA-mediated knockdown
Primary skeletal muscle cells were prepared from 3- to 4-d-old mouse pups. Cells were maintained in tissue culture dishes coated with Matrigel matrix (Corning, France) in basal medium with 20% fetal bovine serum (FBS), 50 U/ml penicillin, 50 mg/ml streptomycin (growth medium), and 1% chicken embryo extract (Seralab, UK). Differentiation was induced when cells were ~80% confluent by switching to differentiation medium (basal medium with 2% horse serum).
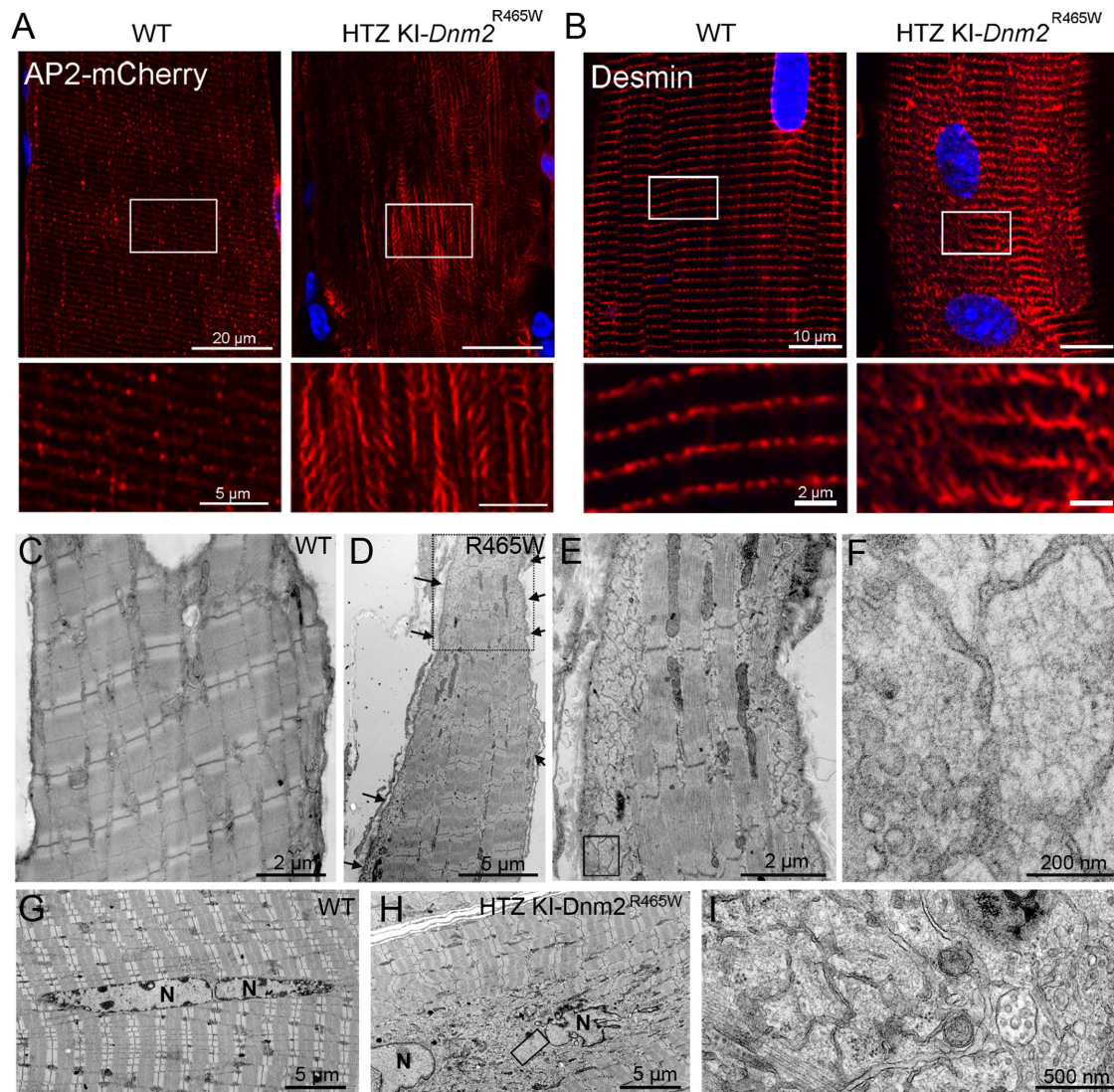
FIGURE 6: Desmin IF defects in HTZ KI-*Dnm2* [R465W] mice. (A) AP2 mCherry distribution between WT and HTZ KI-*Dnm2*[R465W] mice at the surface of myofibers on longitudinal muscle cryosections. (B) Confocal sections from the surface of WT (left panel) or HTZ KI-*Dnm2* [R465W] (right panel) mouse dissociated skeletal muscle fibers immunolabeled with desmin antibody. Images are representative of at least three independent experiments. (C–F) Thin-section EM of surface longitudinal skeletal muscle sections from either WT (C) or HTZ KI-*Dnm2* [R465W] (D–F) mice. The presence of desmin filament aggregates at the periphery of the fiber are clearly visible on the insets. (G–I) Longitudinal skeletal muscle sections from the core of either WT (G) or HTZ KI-*Dnm2* [R465W] mice (H, I) displaying central nuclei. The presence of desmin filament aggregates around myonuclei is visible in the inset (I).

To avoid detachment due to strong contractions and to keep cells in culture for prolonged periods of differentiation, myotubes were covered with a layer of Matrigel Growth Factor Reduced Basement Membrane Matrix, Phenol Red-Free (Corning, France) (Falcone *et al.*, 2014). For siRNA treatment, cells (differentiated for either 4 or 6 d) were transfected twice for 48 h using 200 nM siRNA and HiPerfect transfection reagent (Qiagen, Germany) according to the manufacturer's instructions. Targeting and control siRNAs were synthesized by Eurogentec, Belgium. A list of siRNAs used and sequences can be found in Supplemental Table 1. Targeted sequences for CHC, AP2, and DNM2 were previously published (Ezratty *et al.*, 2009; Vassilopoulos *et al.*, 2014).

EM of unroofed myotubes

Adherent PMs from cultured cells grown on glass coverslips were obtained by sonication as described previously (Heuser, 2000).

Sample processing for platinum-replica EM of unroofed cells was performed as follows: 2% glutaraldehyde/2% paraformaldehyde-fixed cells were further sequentially treated with 0.5% OsO$_4$, 1% tannic acid, and 1% uranyl acetate before graded ethanol dehydration and hexamethyldisilazane substitution (Sigma-Aldrich, France). For immunogold labeling, 4% paraformaldehyde-fixed PMs were washed and quenched before incubation with primary and 15 nm gold-coupled secondary antibodies and further fixed with 2% glutaraldehyde. Dried samples were then rotary shadowed with 2 nm of platinum and 5–8 nm of carbon using an ACE600 metal coater (Leica Microsystems, Germany). The resultant platinum replica was floated off the glass with hydrofluoric acid (5%), washed several times on distilled water, and picked up on 200 mesh formvar/carbon-coated EM grids. The grids were mounted in a eucentric side-entry goniometer stage of a transmission electron microscope operated at 80 kV (model CM120; Philips), and images were recorded with a Morada digital camera
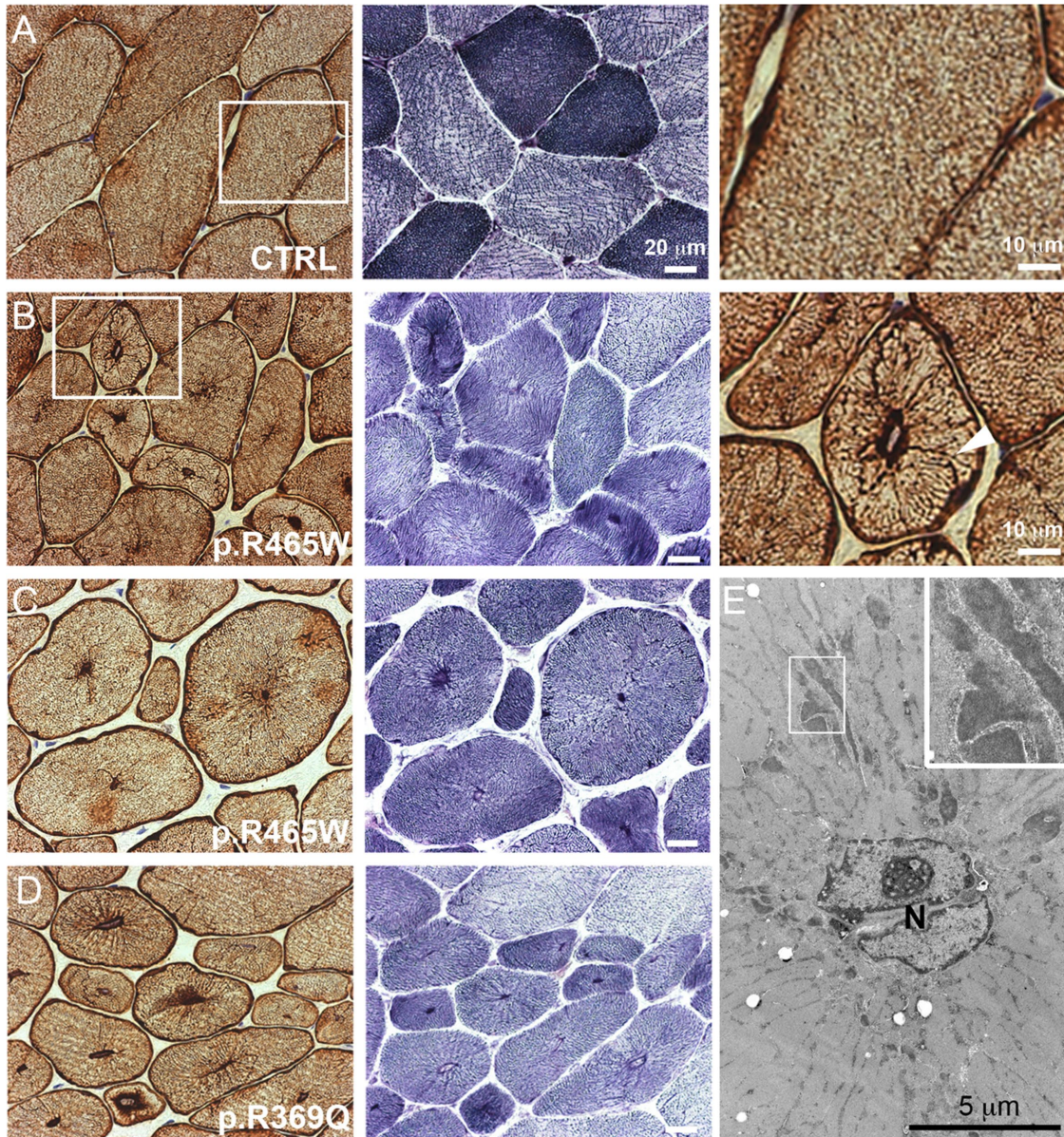
FIGURE 7: Desmin IF defects in human CNM patients. (A–D) Muscle biopsy sections of a control patient (A), two patients with p.R465W DNM2 mutation (B, C), and one patient with p.R369Q DNM2 mutation (D) were either immunohistochemically labeled against desmin or stained with NADH-TR reaction C. Muscle sections from the patient reveal a strong desmin labeling of radial sarcoplasmic strands. NADH-TR reaction C on muscle section from CNM patients displays a high percentage of small rounded fibers with centralized nuclei and few fibers with typical radiating sarcoplasmic strands. Radial desmin labeling is indicated with arrowheads in B. Note that desmin labeling continuously extends from the central nucleus to the sarcolemma. (E) Thin-section EM of muscle from a CNM patient with the p. R465W mutation presenting characteristic radial strands. Note the dilated Z-band material in the inset.

(Olympus, Tokyo). Images were processed in Adobe Photoshop to adjust brightness and contrast and presented in inverted contrast. Anaglyphs were made by converting the −10° tilt image to red and the +10° tilt image to cyan (blue/green), layering them on top of each other using the screen blending mode in Adobe Photoshop, and aligning them to each other. Tomograms were made by collecting images at the tilt angles up to ±25° relative to the plane of the sample with 5° increments. Images were aligned by layering them on top of each other in Adobe Photoshop. Clathrin structure morphometric analysis from unroofed PMs was performed using ImageJ software (Schindelin *et al.*, 2012) by manually counting and measuring pit and plaque areas normalized to the total membrane area.

Dissociated fibers
Myofibers were isolated by mechanical dissociation from the dissected TA muscle of 3- or 7-mo-old mice fixed 48 h in 4% paraformaldehyde.

Immunofluorescence microscopy
Adult mouse skeletal muscle was embedded in Tissue-Tek OCT compound (Miles), frozen, and stored at −80°C. Cryosections (10 µm thick) were fixed (15 min, 4% paraformaldehyde in phosphate-buffered saline [PBS]) at room temperature (RT), permeabilized (10 min, 0.5% Triton X-100 in PBS, RT), and blocked (30 min, PBS with 0.1% Triton X-100, 5% bovine serum albumin [BSA]).

Sections were incubated with primary antibodies (overnight, 4°C, in PBS with 0.1% Triton X-100, 5% BSA), and washed in PBS with 0.1% Triton X-100. Sections were then incubated with secondary antibodies (60 min, RT), washed in PBS with 0.1% Triton X-100, and mounted with Vectashield anti-fading solution containing 4′,6-diamidino-2-phenylindole (DAPI; Vector Laboratories, USA). For double or triple labeling, the primary antibodies (from different species) were added simultaneously at the appropriate step.

For mouse and human cells grown on coverslips, cells were washed in warm PBS, fixed in paraformaldehyde (4% in PBS, 15 min), and then washed in PBS, permeabilized (10 min, 0.5% Triton X-100 in PBS), and blocked (5% BSA in PBS with 0.1% Triton X-100, 30 min). Antibody labeling was performed by addition of 200 µl blocking solution with primary or secondary antibodies and washing with PBS with 0.1% Triton X-100. F-actin was stained using Alexa Fluor 555 Phalloidin for 1 h at RT. Samples were mounted in Vectashield containing DAPI (Vector Laboratories, USA).

Samples were analyzed by confocal laser-scanning microscopy using an upright FV-1000 confocal laser-scanning microscope (Olympus, Tokyo) equipped with UPlanS-Apo 60×/1.35 NA oil-immersion objective lenses or an SP5 inverted microscope (Leica, Germany) equipped with a Leica HyD hybrid detector. DAPI, Alexa Fluor 488, and Alexa Fluor 568 were sequentially excited using lasers with wavelengths of 405 for DAPI, 473 for Alexa Fluor 488, and 543 nm for Alexa Fluor 568. Z-series from the top to the bottom of fibers were sequentially collected for each channel with a step of 0.8–1 µm between each frame. Imaging was performed at RT using Leica Type F immersion oil. Images (1024 × 1024 pixels) were saved as TIFF files in OLYMPUS FV-1000 software, and levels were adjusted in Adobe Photoshop. Image quantification was performed using National Institutes of Health's FIJI (Schindelin et al., 2012).

Immunoblot analysis

Cell samples were collected using Laemmli blue 4X directly or an NaCl (150 mM)-EDTA (10 mM) buffer with added proteinase inhibitor cocktail (Sigma-Aldrich, France). Protein samples were separated by electrophoresis (4–12% bis-acrylamide gel; Life Technologies, France) and then electrophoretically transferred to 0.45 µm nitrocellulose membranes (Life Technologies, France) and labeled with primary antibodies and secondary antibodies coupled to HRP. The presence of proteins in samples was detected using Immobilon Western Chemiluminescent HRP Substrate (Sigma-Aldrich, France). Acquisition was performed on a G-Box (Ozyme, France).

Immunoprecipitation

Immunoprecipitations were performed on primary cell cultures. Myotube pellets were resuspended in 500 µl of lysis buffer (50 mM Tris-HCl, pH 7.5, 0.15 M NaCl, 1 mM EDTA, 1% NP-40) and protein inhibitor cocktail 1:100 (Sigma Aldrich, France). The protocol was modified to reduce nonspecific binding of desmin on the beads. Each sample (200–500 µg) was precleared twice with 30 µl protein G–Sepharose (PGS 4 Fast Flow; ThermoFisher, France) and incubated with 20 µg of specific antibody overnight (4°C). Washed PGS (40 µl) was first incubated with BSA (2 g/l) and further incubated with samples for 2 h at 4°C. Pelleted PGS was taken up in sample buffer and subjected to electrophoresis and immunoblotting. For all immunoprecipitation experiments, HRP-conjugated rabbit and mouse IgG TrueBlot secondary antibodies (Rockland, USA) were used.

AAV production, titration, and in vivo gene transfer

An AAV serotype 9 was produced for expression of the µ2-subunit of the AP2 clathrin adaptor tagged with mCherry (AP2-mCherry) (Taylor et al., 2011). AAV2/9 pseudotyped vectors were prepared by tri-transfection in 293 cells as described previously (Rivière et al., 2006) using the pSMD2-AP2-mCherry plasmid, pXX6 plasmid coding for the viral sequences essential for AAV production, and the pRepCap plasmid coding for serotype 9 capsid. Vector particles were purified on iodixanol gradient and concentrated on Amicon Ultra-15 100K columns (Merck-Millipore, USA). The viral genomes titer (vg/ml) was determined by quantitative real-time PCR. WT and HTZ KI-Dnm2^{R465W} mice were injected at 6 mo of age. One intramuscular injection (40 µl/TA) of AAV9-AP2-mCherry at 6.10^{11} vg/ml was performed in TA muscles using a 29G needle.

Histomorphological and ultrastructural analyses

Human open-muscle biopsies from two patients carrying the CNM-DNM2 mutation p.R465W, one patient carrying the CNM-DNM2 mutation p.R369Q, and two healthy control muscles were performed at the Centre de Référence de Pathologie Neuromusculaire Paris-Est, Institut de Myologie, Assistance Publique-Hôpitaux de Paris, GH Pitié-Salpêtrière, Paris, France, following written informed consent specially dedicated for diagnosis and research. Muscle was frozen in liquid nitrogen–cooled isopentane. For conventional histochemical techniques on human biopsies, 10-µm-thick cryostat sections were stained with antibodies against desmin, with reduced nicotinamide adenine dinucleotide dehydrogenase-tetrazolium reductase (NADH-TR) by standard methods. Pictures of each section were obtained with a Zeiss AxioCam HRc linked to a Zeiss Axioplan bright-field microscope and processed with the Axio Vision 4.4 software (Zeiss, Germany).

For thin-section EM, mouse muscles were fixed by intra-aortic perfusion with 2% paraformaldehyde and 2% glutaraldehyde in 0.1 M phosphate buffer (pH 7.4). TA samples were postfixed with 2% OsO$_4$ in 0.1 M phosphate buffer (pH 7.4) for 1 h and then dehydrated in a graded acetone series, including a 1% uranyl acetate staining step in 70% acetone, and finally embedded in epoxy resin (EMBed-812; Electron Microscopy Sciences, USA). Myotubes grown on Thermanox coverslips (Nunc, Rochester, USA) were directly fixed for 30 min in the same fixation solution and processed as previously indicated for TA muscles. Ultrathin (70 nm) sections were stained with uranyl acetate and lead citrate. For patient biopsies, frozen muscle sections (40 µm) were fixed in osmium tetroxide (1%), dehydrated, and embedded in epoxy resin (as described earlier). Ultrathin (80 nm) sections were stained with uranyl acetate and lead citrate. Observations were made on a Philips CM120 electron microscope operated at 80 kV (Philips, Eindhoven, The Netherlands), and images were recorded with a Morada digital camera (Olympus Soft Imaging Solutions GmbH, Münster, Germany).

Image analysis

Desmin aggregate size analysis was achieved using the Analyze Particles FIJI plug-in (v. 1.46) to count intracellular particles on binary confocal images of primary mouse myotubes in a single image from the middle of the cell. The same treatment was used to measure the size of clathrin plaques on confocal images and cortical actin. Fluorescence was measured on confocal images using this formula:

$$\text{Corrected total cell fluorescence (CTCF)}$$
$$= \text{Integrated density} - (\text{Area of selected region of interest}$$
$$\times \text{Mean fluorescence of background reading})$$

Data analysis and statistics

Graphics and statistical analyses were performed with Excel and GraphPad Prism v. 5.00 software. Statistical analysis was performed using Student's *t* test. Values are expressed as means ± SEM. The number of samples (*n*), representing the number of independent biological replicates, is indicated in the figure legends. Statistical comparisons between two groups were performed using unpaired one- or two-tailed Student's *t* tests as specified. Statistical tests applied are indicated in the figure legends. $p < 0.05$ was considered statistically significant.

Study approval

Animal studies conform to the French laws and regulations concerning the use of animals for research and were approved by an external ethics committee (approval no. 00351.02 delivered by the French Ministry of Higher Education and Scientific Research). For human studies, all individuals provided informed consent for muscle biopsies according to a protocol approved by the ethics committee of the Centre de Référence de Pathologie Neuromusculaire Paris-Est, Institut de Myologie, Assistance Publique-Hôpitaux de Paris, GH Pitié-Salpêtrière, Paris, France.

Data availability

All data supporting the findings of this study are available from the corresponding author on request.

REFERENCES

Bitoun M, Maugenre S, Jeannet PY, Lacène E, Ferrer X, Laforêt P, Martin JJ, Laporte J, Lochmüller H, Beggs AH, *et al.* (2005). Mutations in dynamin 2 cause dominant centronuclear myopathy. Nat Genet 37, 1207–1209.

Bonazzi M, Kühbacher A, Toledo-Arana A, Mallet A, Vasudevan L, Pizarro-Cerdá J, Brodsky FM, Cossart P (2012). A common clathrin-mediated machinery co-ordinates cell-cell adhesion and bacterial internalization. Traffic 13, 1653–1666.

Brodsky FM (2012). Diversity of clathrin function: new tricks for an old protein. Annu Rev Cell Dev Biol 28, 309–336.

Capetanaki Y, Papathanasiou S, Diokmetzidou A, Vatsellas G, Tsikitis M (2015). Desmin related disease: a matter of cell survival failure. Curr Opin Cell Biol 32, 113–120.

Chorev DS, Moscovitz O, Geiger B, Sharon M (2014). Regulation of focal adhesion formation by a vinculin-Arp2/3 hybrid complex. Nat Commun 5, 3758.

Clemen CS, Stöckigt F, Strucksberg KH, Chevessier F, Winter L, Schütz J, Bauer R, Thorweihe JM, Wenzel D, Schlötzer-Schrehardt U, *et al.* (2015). The toxic effect of R350P mutant desmin in striated muscle of man and mouse. Acta Neuropathol (Berl) 129, 297–315.

Collins A, Warrington A, Taylor KA, Svitkina T (2011). Structural organization of the actin cytoskeleton at sites of clathrin-mediated endocytosis. Curr Biol 21, 1167–1175.

Dambournet D, Sochacki KA, Cheng AT, Akamatsu M, Taraska JW, Hockemeyer D, Drubin DG (2018). Genome-edited human stem cells expressing fluorescently labeled endocytic markers allow quantitative analysis of clathrin-mediated endocytosis during differentiation. J Cell Biol 217, 3301–3311.

Damke H, Baba T, Warnock DE, Schmid SL (1994). Induction of mutant dynamin specifically blocks endocytic coated vesicle formation. J Cell Biol 127, 915–934.

Danowski BA, Imanaka-Yoshida K, Sanger JM, Sanger JW (1992). Costameres are sites of force transmission to the substratum in adult rat cardiomyocytes. J Cell Biol 118, 1411–1420.

De Deyne PG, O'Neill A, Resneck WG, Dmytrenko GM, Pumplin DW, Bloch RJ (1998). The vitronectin receptor associates with clathrin-coated membrane domains via the cytoplasmic domain of its beta5 subunit. J Cell Sci 111, 2729–2740.

Durieux A-C, Vignaud A, Prudhon B, Viou MT, Beuvin M, Vassilopoulos S, Fraysse B, Ferry A, Lainé J, Romero NB, *et al.* (2010). A centronuclear myopathy-dynamin 2 mutation impairs skeletal muscle structure and function in mice. Hum Mol Genet 19, 4820–4836.

Ervasti JM (2003). Costameres: the Achilles' heel of Herculean muscle. J Biol Chem 278, 13591–13594.

Ezratty EJ, Bertaux C, Marcantonio EE, Gundersen GG (2009). Clathrin mediates integrin endocytosis for focal adhesion disassembly in migrating cells. J Cell Biol 187, 733–747.

Falcone S, Roman W, Hnia K, Gache V, Didier N, Lainé J, Auradé F, Marty I, Nishino I, Charlet-Berguerand N, *et al.* (2014). N-WASP is required for amphiphysin-2/BIN1-dependent nuclear positioning and triad organization in skeletal muscle and is involved in the pathophysiology of centronuclear myopathy. EMBO Mol Med 6, 1455–1475.

González-Jamett AM, Baez-Matus X, Olivares MJ, Hinostroza F, Guerra-Fernández MJ, Vasquez-Navarrete J, Bui MT, Guicheney P, Romero NB, Bevilacqua JA, *et al.* (2017). Dynamin-2 mutations linked to centronuclear myopathy impair actin-dependent trafficking in muscle cells. Sci Rep 7, 4580.

Grove J, Metcalf DJ, Knight AE, Wavre-Shapton ST, Sun T, Protonotarios ED, Griffin LD, Lippincott-Schwartz J, Marsh M (2014). Flat clathrin lattices: stable features of the plasma membrane. Mol Biol Cell 25, 3581–3594.

Gu C, Yaddanapudi S, Weins A, Osborn T, Reiser J, Pollak M, Hartwig J, Sever S (2010). Direct dynamin-actin interactions regulate the actin cytoskeleton. EMBO J 29, 3593–3606.

Herrmann H, Bär H, Kreplak L, Strelkov SV, Aebi U (2007). Intermediate filaments: from cell architecture to nanomechanics. Nat Rev Mol Cell Biol 8, 562–573.

Heuser J (1980). Three-dimensional visualization of coated vesicle formation in fibroblasts. J Cell Biol 84, 560–583.

Heuser J (2000). The production of "cell cortices" for light and electron microscopy. Traffic 1, 545–552.

Kaksonen M, Roux A (2018). Mechanisms of clathrin-mediated endocytosis. Nat Rev Mol Cell Biol 19, 313–326.

Kaksonen M, Toret CP, Drubin DG (2006). Harnessing actin dynamics for clathrin-mediated endocytosis. Nat Rev Mol Cell Biol 7, 404–414.

Lampe M, Vassilopoulos S, Merrifield C (2016). Clathrin coated pits, plaques and adhesion. J Struct Biol 196, 48–56.

Leyton-Puig D, Isogai T, Argenzio E, van den Broek B, Klarenbeek J, Janssen H, Jalink K, Innocenti M (2017). Flat clathrin lattices are dynamic actin-controlled hubs for clathrin-mediated endocytosis and signalling of specific receptors. Nat Commun 8, 16068.

Maupin P, Pollard TD (1983). Improved preservation and staining of HeLa cell actin filaments, clathrin-coated membranes, and other cytoplasmic structures by tannic acid-glutaraldehyde-saponin fixation. J Cell Biol 96, 51–62.

Merrifield CJ, Qualmann B, Kessels MM, Almers W (2004). Neural Wiskott Aldrich syndrome protein (N-WASP) and the Arp2/3 complex are recruited to sites of clathrin-mediated endocytosis in cultured fibroblasts. Eur J Cell Biol 83, 13–18.

Orth JD, McNiven MA (2003). Dynamin at the actin-membrane interface. Curr Opin Cell Biol 15, 31–39.

Palmisano MG, Bremner SN, Hornberger TA, Meyer GA, Domenighetti AA, Shah SB, Kiss B, Kellermayer M, Ryan AF, Lieber RL (2015). Skeletal muscle intermediate filaments form a stress-transmitting and stress-signaling network. J Cell Sci 128, 219–224.

Pardo JV, Siliciano JD, Craig SW (1983a). A vinculin-containing cortical lattice in skeletal muscle: transverse lattice elements ("costameres") mark

sites of attachment between myofibrils and sarcolemma. Proc Natl Acad Sci USA 80, 1008–1012.

Pardo JV, Siliciano JD, Craig SW (1983b). Vinculin is a component of an extensive network of myofibril-sarcolemma attachment regions in cardiac muscle fibers. J Cell Biol 97, 1081–1088.

Pizarro-Cerdá J, Chorev DS, Geiger B, Cossart P (2017). The diverse family of Arp2/3 complexes. Trends Cell Biol 27, 93–100.

Rivière C, Danos O, Douar AM (2006). Long-term expression and repeated administration of AAV type 1, 2 and 5 vectors in skeletal muscle of immunocompetent adult mice. Gene Ther 13, 1300–1308.

Robinson MS (2015). Forty years of clathrin-coated vesicles. Traffic 16, 1210–1238.

Roman W, Martins JP, Carvalho FA, Voituriez R, Abella JVG, Santos NC, Cadot B, Way M, Gomes ER (2017). Myofibril contraction and crosslinking drive nuclear movement to the periphery of skeletal muscle. Nat Cell Biol 19, 1189–1201.

Saffarian S, Cocucci E, Kirchhausen T (2009). Distinct dynamics of endocytic clathrin-coated pits and coated plaques. PLoS Biol 7, e1000191.

Schafer DA, Weed SA, Binns D, Karginov AV, Parsons JT, Cooper JA (2002). Dynamin2 and cortactin regulate actin assembly and filament organization. Curr Biol 12, 1852–1857.

Schindelin J, Arganda-Carreras I, Frise E, Kaynig V, Longair M, Pietzsch T, Preibisch S, Rueden C, Saalfeld S, Schmid B, et al. (2012). Fiji: an open-source platform for biological-image analysis. Nat Methods 9, 676–682.

Shear CR, Bloch RJ (1985). Vinculin in subsarcolemmal densities in chicken skeletal muscle: localization and relationship to intracellular and extracellular structures. J Cell Biol 101, 240–256.

Sochacki KA, Dickey AM, Strub M-P, Taraska JW (2017). Endocytic proteins are partitioned at the edge of the clathrin lattice in mammalian cells. Nat Cell Biol 19, 352–361.

Taylor MJ, Perrais D, Merrifield CJ (2011). A high precision survey of the molecular dynamics of mammalian clathrin-mediated endocytosis. PLoS Biol 9, e1000604.

van Dam EM, Stoorvogel W (2002). Dynamin-dependent transferrin receptor recycling by endosome-derived clathrin-coated vesicles. Mol Biol Cell 13, 169–182.

Vassilopoulos S, Gentil C, Lainé J, Buclez PO, Franck A, Ferry A, Précigout G, Roth R, Heuser JE, Brodsky FM, et al. (2014). Actin scaffolding by clathrin heavy chain is required for skeletal muscle sarcomere organization. J Cell Biol 205, 377–393.

Warnock DE, Baba T, Schmid SL (1997). Ubiquitously expressed dynamin-II has a higher intrinsic GTPase activity and a greater propensity for self-assembly than neuronal dynamin-I. Mol Biol Cell 8, 2553–2562.

Yarar D, Waterman-Storer CM, Schmid SL (2005). A dynamic actin cytoskeleton functions at multiple stages of clathrin-mediated endocytosis. Mol Biol Cell 16, 964–975.

Zuidema A, Wang W, Kreft M, Te Molder L, Hoekman L, Bleijerveld OB, Nahidiazar L, Janssen H, Sonnenberg A (2018). Mechanisms of integrin αVβ5 clustering in flat clathrin lattices. J Cell Sci 131, jcs221317.